Mixed Layer Deepening Due to Langmuir Circulation

MING LI AND CHRIS GARRETT

Centre for Earth and Ocean Research, University of Victoria, Victoria, British Columbia, Canada

(Manuscript received 27 March 1996, in final form 28 May 1996)

ABSTRACT

The interaction between wind-driven Langmuir circulation and preexisting stratification is examined in order to elucidate its role in the deepening of the ocean surface mixed layer. For linear stratification, a numerical model suggests that Langmuir cells initially engulf water and create a homogeneous surface layer. The depth $\tilde{h}$ of this layer can be understood in terms of a Froude number $\mathrm{Fr} = \tilde{w}_{dn}/(N\tilde{h})$, where $\tilde{w}_{dn}$ is the maximum downwelling velocity generated by Langmuir circulation in homogeneous water and N is the buoyancy frequency. Numerical results show that Fr is a constant ≈ 0.6. Using computed values of $\tilde{w}_{dn}$, this implies that the rapid mixed layer deepening stops at $\tilde{h} = cu_*/N$ in which u_* is the water friction velocity and the coefficient c is about 10 for fully developed seas. Alternatively, the deepening is arrested when the buoyancy jump Δb at the mixed layer base reaches about $50u_*^2/\tilde{h}$. The above formula, compared with the Price, Weller, and Pinkel value of 0.65 for the bulk Richardson number R_b associated with shear mixing, suggests that engulfment by Langmuir circulation dominates mixed layer deepening if the velocity difference $|\Delta\tilde{\mathbf{u}}|$ across the base of the mixed layer is less than about $0.01U_w$, where U_w is the wind speed. The buoyancy jump criterion is tested for two-layer stratification profiles and found to be a robust formula suitable for incorporation into one-dimensional mixed layer models.

The possibility of further mixed layer deepening through shear instability is studied by examining the distribution of the gradient Richardson number Ri_g, particularly in a transition region beneath the mixed layer. It has great variability across wind, reaching minimum values beneath downwelling jets, but can fall below 0.25, indicating the onset of shear instability. Thus, Langmuir cells may facilitate shear instability in a horizontally confined region beneath downwelling jets, although further study will require allowance for a different background shear.

1. Introduction

When the wind blows across a stratified ocean, a surface mixed layer (SML) develops in which the density is approximately uniform. The lower boundary is marked by a strongly stratified transition region. The density jump across this increases as the mixed layer deepens.

Shear-driven turbulence may contribute to the mixing and density homogenization in the SML during wind events, but another important process is wind-driven Langmuir circulation (LC). This consists of a pattern of fairly parallel vortices oriented downwind, with alternating vorticity and maximum downwind surface current at the surface convergences. Following a series of ingenious experiments, Langmuir (1938) suggested that the circulation patterns constitute the essential mechanism by which the mixed layer is produced. Recent observations by Weller and Price (1988) showed a downward vertical velocity sometimes exceeding 0.2 m s^{-1}. Langmuir circulation appeared to rapidly mix away shallow near-surface stratification associated with diurnal heating, within one-third to one-half of the original SML depth, but they found no evidence that LC played a direct role in mixing near the base of the nighttime 40–60 m SML present during the experiment. No quantitative criterion for the effect of LC was suggested.

Thus, despite Langmuir's pioneering paper over five decades ago, the role of LC in distributing heat and momentum in the upper ocean or in forming the seasonal thermocline is not yet determined (Thorpe 1985, 1992). Moreover, none of the existing mixed layer models have explicitly taken LC into consideration.

Most mixed layer models are one-dimensional and assume that the mean temperature and horizontal velocity are quasi-uniform within the layer but have a jump at the lower boundary. To close the model, the entrainment velocity at the SML base is prescribed in terms of the wind stress and/or the difference of the velocity and density between the mixed layer and the water below it (Niiler and Kraus 1977; Price et al. 1986). These bulk models, as well as more elaborate higher-order turbulence closure models (e.g., Mellor and Yamada 1974, 1982; Large et al. 1994), suffer from not explicitly incorporating the key physical processes in the ocean

Corresponding author address: Dr. Ming Li, Institute of Ocean Studies, P.O.Box 6000, 9860 West Saanich Rd., Sidney, BC V8L 4B2, Canada.
E-mail: mli@ios.bc.ca

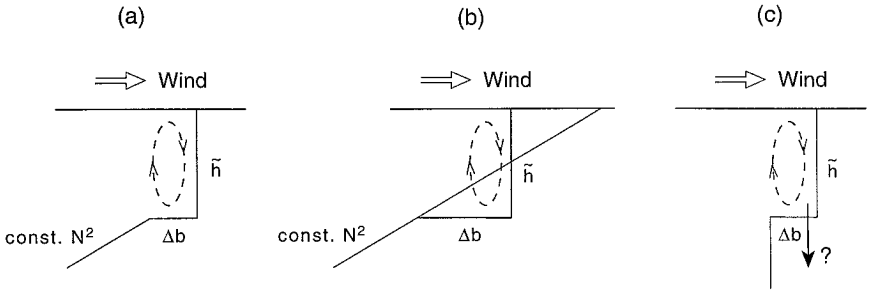

FIG. 1. Schematic diagram showing the interaction between Langmuir circulation and three kinds of preexisting stratification. (a) General stratification, (b) linear stratification, and (c) two-layer stratification.

surface layer that are responsible for the SML deepening, and it is not at all clear that their parameterization implicitly models these processes correctly.

This paper investigates the role of wind-driven LC in the deepening of the ocean SML. The model we use to simulate LC is that of Craik and Leibovich (Craik 1977; Leibovich 1977) in which the Stokes drift of surface waves tilts the vertical vortex lines of a near-surface downwind jet to produce streamwise vorticity with surface convergence at the jet maximum. The jet is then reinforced by continued acceleration, by the wind stress, of the converging surface flow. Li and Garrett (1995, hereafter LG95) confirm that the vortex force associated with the Stokes drift is powerful, dominating over the buoyancy force in driving the circulation for typical values of wind, waves, and surface buoyancy flux.

Figure 1a illustrates the problem under consideration. A mixed layer with depth $\tilde{h}$ and a buoyancy jump Δb at its base lies above uniformly stratified deep water, which has a buoyancy frequency N. There is a surface wind stress $\tau = \rho_w u_*^2$, where ρ_w is the water density and u_* is the water friction velocity. The Stokes drift is usually approximated by an exponential profile in the LC model; that is, $\tilde{u}_s = 2S_0 e^{2\beta\tilde{z}}$ in which $2S_0$ is the surface drift velocity and $1/(2\beta)$ is the e-folding depth (e.g., Li and Garrett 1993, hereafter LG93). Small-scale mixing is parameterized in terms of eddy viscosity ν_T and eddy diffusivity κ_T. Our question is whether and how LC deepens the mixed layer. Dimensional analysis shows that six dimensionless parameters control the flow: 1) the Langmuir number $\mathrm{La} = (\nu_T\beta/u_*)^{3/2}(S_0/u_*)^{-1/2}$, which is a ratio of viscous to inertial forces (Leibovich 1977; LG93); 2) the Prandtl number $\mathrm{Pr} = \nu_T/\kappa_T$; 3) $R_{Lb} = \Delta b\nu_T/(S_0 u_*^2)$, measuring the strength of the buoyancy jump at the mixed layer base; 4) $R_{LN} = N^2\nu_T/(S_0\beta u_*^2)$, describing stratification in deep water; 5) the length scale ratio $\beta\tilde{h}$, comparing the surface layer depth with the e-folding depth of the Stokes drift; and 6) the ratio $S_w = S_0/u_*$, representing the ratio of surface Stokes drift to water friction velocity. One can rewrite $R_{Lb} = 4\beta\Delta b/(S_{\mathrm{Stokes}}S_{\mathrm{mean}})$ and $R_{LN} = 4N^2/(S_{\mathrm{Stokes}}S_{\mathrm{mean}})$, where $S_{\mathrm{Stokes}} = 4S_0\beta$ is the surface shear in the Stokes drift current and $S_{\mathrm{mean}} = u_*^2/\nu_T$ is the shear in the wind-driven current. Thus, both R_{Lb} and R_{LN} can be seen as Richardson numbers.

We shall examine the problem for an appropriate range of La, R_{Lb}, and R_{LN} and for $\mathrm{Pr} = 1$ or 2. The ratio S_w does not occur explicitly in the nondimensionalized equations governing the problem and only affects the scaling back to dimensional variables. Based on numerical results, we shall argue that the mixed layer deepening is independent of $\beta\tilde{h}$ since $e^{2\beta\tilde{h}}$ is normally much greater than 1 so that the vortex force due to the Stokes drift is concentrated near the surface.

We shall examine two simplified models. In the first model, there is a preexisting linear stratification (Fig. 1b) for which the buoyancy content of the water is conserved so that $R_{Lb} = R_{LN}(\beta\tilde{h})/2$, but we will examine a range of R_{LN} values. In the second model, the water consists of two homogeneous layers connected by a sharp interface (Fig. 1c). We then have $R_{LN} = 0$ but R_{Lb} will be varied across an appropriate range. The similarity of the results obtained for the two simple models, and supporting physical arguments, will suggest that the criterion we derive for mixed layer deepening by LC is applicable to the general model illustrated in Fig. 1a.

2. A model for LC eroding linear stratification

Leibovich and Paolucci (1980) developed a model to study the interaction between LC and a preexisting linear stratification. They fixed the temperature at the top and bottom boundaries of the computational domain so that, with more stirring near the surface, there was a net heat flux into the water column. Moreover, a programming error in their computer code rendered the numerical solutions strictly valid only when temperature was a passive scalar (Leibovich 1983). This programming error was later corrected by Lele (1985), who also considered LC interacting with stratification profiles more appropriate to the ocean. Lele showed that stratification can be broken down by LC, but he did not propose any quantitative criterion for SML deepening and also retained the fixed temperature boundary condition.

We propose a different starting point. The water column at rest is assumed to be uniformly stratified with

buoyancy frequency N. We maintain this stratification by a constant downward heat flux $Q = C_p\rho_w\kappa_T\partial\tilde{\theta}/\partial\tilde{z} = C_p\rho_w\kappa_T N^2/(\alpha g)$ through the surface to balance the heat loss through the bottom boundary and conserve the total heat content of the water column, though the magnitude of the flux is small enough to be dynamically unimportant (LG95). Here C_p is the specific heat at constant pressure, ρ_w the water density, κ_T the eddy diffusivity of heat, α the coefficient of thermal expansion, and $\tilde{\theta}$ the temperature. We then impose a surface wind stress τ and see how cells grow from random noise and erode the stratification.

The dimensional governing equations are (Leibovich 1977)

$$\frac{\partial\tilde{u}}{\partial\tilde{t}} + \tilde{v}\frac{\partial\tilde{u}}{\partial\tilde{y}} + \tilde{w}\frac{\partial\tilde{u}}{\partial\tilde{z}} = \nu_T\nabla^2\tilde{u}, \tag{1}$$

$$\frac{\partial\tilde{\Omega}}{\partial\tilde{t}} + \tilde{v}\frac{\partial\tilde{\Omega}}{\partial\tilde{y}} + \tilde{w}\frac{\partial\tilde{\Omega}}{\partial\tilde{z}} = \nu_T\nabla^2\tilde{\Omega} - \frac{d\tilde{u}_s}{d\tilde{z}}\frac{\partial\tilde{u}}{\partial\tilde{y}} + \alpha g\frac{\partial\tilde{\theta}}{\partial\tilde{y}}, \tag{2}$$

$$\frac{\partial\tilde{\theta}}{\partial\tilde{t}} + \tilde{v}\frac{\partial\tilde{\theta}}{\partial\tilde{y}} + \tilde{w}\frac{\partial\tilde{\theta}}{\partial\tilde{z}} = \kappa_T\nabla^2\tilde{\theta}, \tag{3}$$

$$\tilde{v} = -\tilde{\psi}_{\tilde{z}}, \qquad \tilde{w} = \tilde{\psi}_{\tilde{y}},$$

$$\tilde{\Omega} = \nabla^2\tilde{\psi}, \tag{4}$$

in which $\tilde{y}$ is in the crosswind direction; $\tilde{z}$ is vertically upward; $\tilde{u}$, v, $\tilde{w}$ represent the downwind, crosswind, and vertical velocities, respectively; and $\tilde{\Omega}$ is the streamwise vorticity. In this model the effects of turbulence are parameterized by constant eddy viscosity ν_T and constant eddy diffusivity κ_T.

Nondimensionalizing distance, velocities, time, and temperature as

$$(\tilde{y}, \tilde{z}) = \beta^{-1}(y, z), \tag{5}$$

$$\tilde{u} = \frac{u_*^2}{\nu_T\beta}u, \tag{6}$$

$$(\tilde{v}, \tilde{w}) = \frac{u_*^2}{\nu_T\beta}\left(\frac{\nu_T S_0\beta}{u_*^2}\right)^{1/2}(v, w), \tag{7}$$

$$\tilde{t} = \frac{\nu_T}{u_*^2}\left(\frac{\nu_T S_0\beta}{u_*^2}\right)^{-1/2}t, \tag{8}$$

$$\tilde{\theta} = \frac{N^2}{\alpha g\beta}\theta, \tag{9}$$

one obtains the nondimensional governing equations

$$\frac{\partial u}{\partial t} + v\frac{\partial u}{\partial y} + w\frac{\partial u}{\partial z} = \mathrm{La}\nabla^2 u, \tag{10}$$

$$\frac{\partial\Omega}{\partial t} + v\frac{\partial\Omega}{\partial y} + w\frac{\partial\Omega}{\partial z} = \mathrm{La}\nabla^2\Omega - \frac{du_s}{dz}\frac{\partial u}{\partial y} + R_{LN}\frac{\partial\theta}{\partial y}, \tag{11}$$

$$\frac{\partial\theta}{\partial t} + v\frac{\partial\theta}{\partial y} + w\frac{\partial\theta}{\partial z} = \frac{\mathrm{La}}{\mathrm{Pr}}\nabla^2\theta, \tag{12}$$

$$v = -\frac{\partial\Psi}{\partial z}, \qquad w = \frac{\partial\Psi}{\partial y},$$

$$\Omega = \nabla^2\Psi, \tag{13}$$

where the Langmuir number (Leibovich 1977), defined as

$$\mathrm{La} = \left(\frac{\nu_T\beta}{u_*}\right)^{3/2}\left(\frac{S_0}{u_*}\right)^{-1/2}, \tag{14}$$

is the ratio of viscous to inertial forces. The Prandtl number $\mathrm{Pr} = \nu_T/\kappa_T$ is the ratio of eddy viscosity to eddy diffusivity. The parameter $R_{LN} = N^2\nu_T/(S_0\beta u_*^2)$ represents the ratio of the buoyancy force to the vortex force associated with surface waves. It can also be understood as the ratio of the buoyancy force to inertial forces and was termed an overall Richardson number by Leibovich and Paolucci (1980). It is possible to introduce a stratification parameter

$$(R_{LN}\mathrm{La}^{-2/3}) = \frac{N^2}{\beta^2 u_*^2}\left(\frac{S_0}{u_*}\right)^{-2/3}, \tag{15}$$

which characterizes the preexisting stratification without the involvement of eddy diffusivity. Model output can then be discussed in terms of La (representing viscous effects), $R_{LN}\mathrm{La}^{-2/3}$ (representing stratification), and Pr, assuming (as we argue later) that the precise value of $\beta\tilde{h}$ is unimportant provided that $e^{2\beta\tilde{h}}$ is much greater than 1.

LG93 estimated La to be in the neighborhood of 0.01 in order for the model to produce the right prediction for the maximum downwelling velocity. For typical stratification in the upper ocean, N^2 ranges up to $O(10^{-4})$ s^{-2}. The wind stress can be estimated from the drag coefficient and the Stokes drift current can be calculated from the wave spectrum. Taking $u_* = 1.3 \times 10^{-3}U_w$, $1/(2\beta) = 0.12U_w^2/g$, and $S_0/u_* = 5.75$ applicable to fully developed seas (LG93), we find that $(R_{LN}\mathrm{La}^{-2/3}) \approx 10^{-2}U_w^2$. For a wind speed $U_w = 10$ m s^{-1}, this upper bound is about 1. From (15) $R_{LN} < 0.1$ for $\mathrm{La} = 0.03$ (which we use later in an example), small enough for the surface buoyancy forcing to be unimportant (LG95). For developing seas R_{LN} will be somewhat smaller due to the increase of β, though this is partially offset by a decrease of S_0.

To solve Eqs. (10)–(13) numerically, we take $u = U(z, t) + u'(z, t)$ and $\theta = T(z) + \theta'(z, t)$, where

$$U(z, t) = 2(\mathrm{La}t)^{1/2} f(\eta), \qquad \eta = \frac{z}{2(\mathrm{La}t)^{1/2}},$$

$$f(\eta) = \pi^{-1/2} e^{-\eta^2} + \eta \mathrm{erfc}(-\eta), \tag{16}$$

$$T(z) = z + \beta\tilde{d}/2, \tag{17}$$

and $\tilde{d} = d/\beta$ is the depth of the computational box.

The boundary conditions to be satisfied at the top and bottom boundaries are

$$\frac{\partial u'}{\partial z} = 0, \qquad \psi = \frac{\partial^2 \psi}{\partial z^2} = 0, \qquad \frac{\partial \theta'}{\partial z} = 0,$$

$$\text{at } z = 0, -\beta\tilde{d}. \tag{18}$$

The perturbation current is stress free, and the heat flux is held constant at both upper and lower boundaries. We choose the computational box to be sufficiently deep such that the deep water remains stagnant and uniformly stratified; in general, the depth d of the computational box is chosen inversely proportional to R_{LN}.

Periodic boundary conditions are imposed at two lateral boundaries; that is,

$$\psi(y + \beta\tilde{L}) = \psi(y), \qquad u'(y + \beta\tilde{L}) = u'(y),$$
$$\theta'(y + \beta\tilde{L}) = \theta'(y), \tag{19}$$

in which $\tilde{L} = L/\beta$ is the width of the computational box. A main goal of this paper is to determine the vertical penetration depth of Langmuir cells. However, as found in LG93, Langmuir cells in homogeneous water typically fill the computational box regardless of the box size. In stratified water LC will be arrested at a certain depth by stratification, but the vertical cell growth could also be constrained by the prescribed lateral boundary conditions (19). To evaluate this possibility, we later widen the computational box to check that the final cell depth reaches a constant value independent of $\beta\tilde{L}$.

For initial conditions, we begin from a linear temperature profile given in nondimensional form by (17). At $t = 0$ an infinitesimal random noise is imposed in the vorticity field and the wind is switched on to drive the flow. For small values of La, it is found to be more economical to start numerical integrations with $U(z, t_0) > 0$ (this presumably could correspond to a preexisting wind-driven current) because $U(z, t)$ is a thin surface jet at small t and requires high resolution.

The formulated mathematical model is solved numerically using a spectral code described in more detail in LG93 and LG95. The solutions ψ, u', and θ' are expanded as Fourier series in both y and z directions and are chosen so that the imposed boundary conditions are satisfied. The spatial resolution is chosen such that the one-dimensional energy spectra show exponential decay at high wavenumbers. It is found that 128×128 Fourier modes provide adequate resolution for the La regime studied in this paper (generally speaking, high resolution is required at low La).

3. Rapid SML deepening through engulfment

The model is now used to examine the interaction between LC and linear stratification. For illustration, we choose La = 0.03, Pr = 1, and $R_{LN} = 0.05$ so that $R_{LN}\mathrm{La}^{-2/3} \approx 0.5$. The computational box has a size of $\beta\tilde{d} = 4\pi$ and $\beta\tilde{L} = 2\pi$, which is judged to be sufficiently large because a further doubling of $\beta\tilde{L}$ does not yield an increase in the depth of the Langmuir cells.

a. Flow fields

Contours of streamfunction, vorticity, downwind current, and temperature reveal detailed flow structures. They are presented in Fig. 2 for different times during cell development. At $t = 20$ (Fig. 2a) four weak cells appear near the surface and the temperature shows a slight deviation from the linear distribution with depth. The cells gain strength and penetrate deeper with time, meanwhile stirring the upper layer. At $t = 60$ (Fig. 2b) the four cells have merged into two cells, similar to the cell amalgamation found in homogeneous water (Leibovich 1983; LG93). The top isotherm is raised at the upwelling site as cold water is engulfed from below. The two remaining large cells continue to intrude vertically into the stratified water as more cold water is engulfed and mixed, but then approach a quasi-steady state and deepen much more slowly. In the contour plots at $t = 160$ (Fig. 2c), no significant further engulfment is apparent in the temperature field. However, horizontal downwind momentum is transferred down to greater depth because of the continual action of wind stress at the surface.

These snapshots of flow fields illustrate the mechanism by which LC erodes stratification. Langmuir cells penetrate into the stratified water by engulfing cold water and this is mixed with near-surface warmer water to form a surface mixed layer, as shown in the profiles averaged across the Langmuir cells.

b. Vertical profiles

Figure 3 shows the time evolution of the averaged downwind current and temperature as well as their vertical gradients. At $t = 20$ the temperature is approximately a linear function of depth and the downwind current decreases away from the surface. As engulfment proceeds ($t = 60$), the temperature appears to be homogenized in a surface layer, suggesting the creation of a SML by Langmuir cells. In a region beneath the cells, the temperature gradient is larger than the initially prescribed value due to mixing in the surface layer. The current shear is reduced in the middle of the SML. The SML continues to deepen, but at a more gradual rate. In the final quasi-steady state ($t = 160$), we observe a

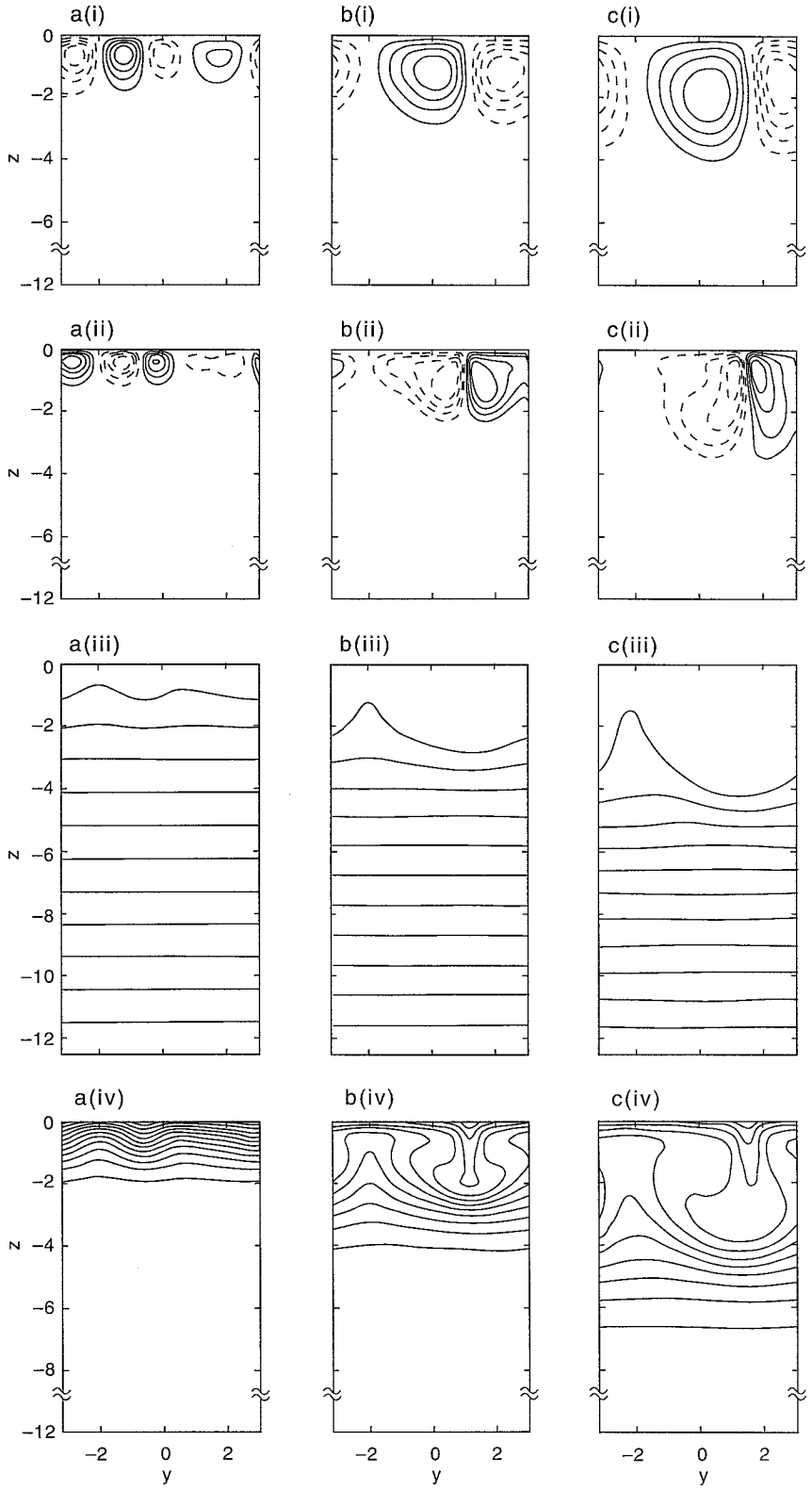

FIG. 2. Contours of (i) streamfunction, (ii) vorticity, (iii) temperature, and (iv) downwind current, for La = 0.03, R_{LN} = 0.05, and Pr = 1, at nondimensional times (a) t = 20, (b) t = 60, and (c) t = 160. The computational box has a size of $\beta\tilde{L} = 2\pi$ and $\beta\tilde{d} = 4\pi$, but we have only shown the full box for temperature. The numerical integration started with $U(z, t_0)$ at t_0 = 10.

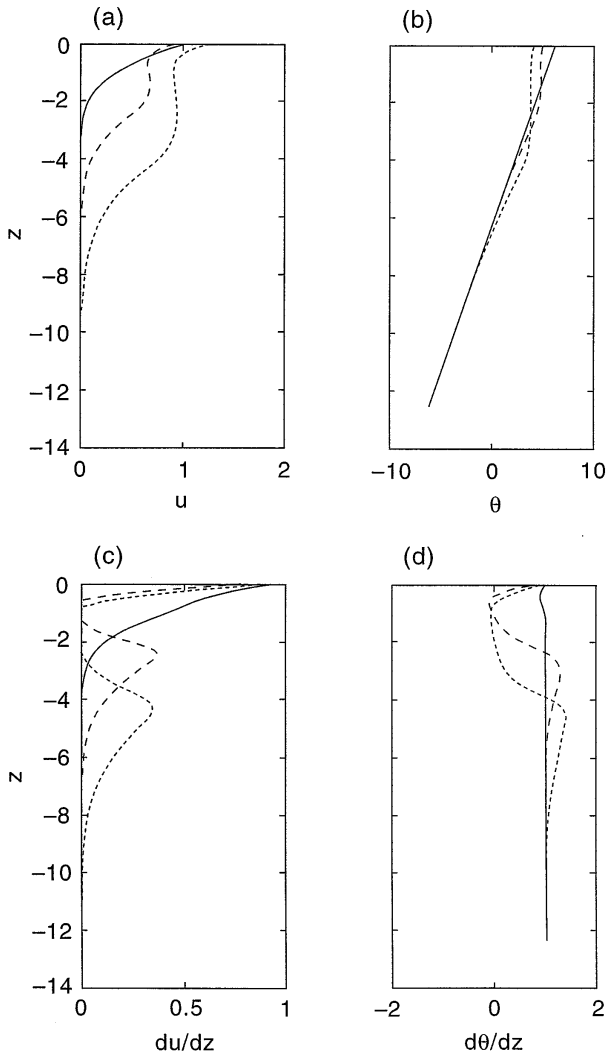

FIG. 3. Vertical profiles of (a) mean downwind current, (b) mean temperature, (c) current shear, and (d) temperature gradient for the same parameters as in Fig. 2 and at times $t = 20$ (solid), $t = 60$ (dashed) and $t = 160$ (short-dashed).

surface layer of fairly uniform temperature and downwind current, above a transition layer with enhanced shear and temperature gradient. In the lower part of the computational box, the water remains uniformly stratified and stagnant.

c. Time series

We define the mixed layer depth $\tilde{h} = h/\beta$ to be the depth of the maximum temperature gradient, averaged across the cells, although, due to the finite background eddy diffusivity, the SML shown in Fig. 3 does not show a sharp jump in temperature across its base. We have experimented with Pr > 1 and observed a more rapid transition with a larger maximum temperature gradient, but with unchanged depth $\beta\tilde{h}$ at which the temperature gradient is maximum.

The mixed layer depth $\beta\tilde{h}$ as a function of time is

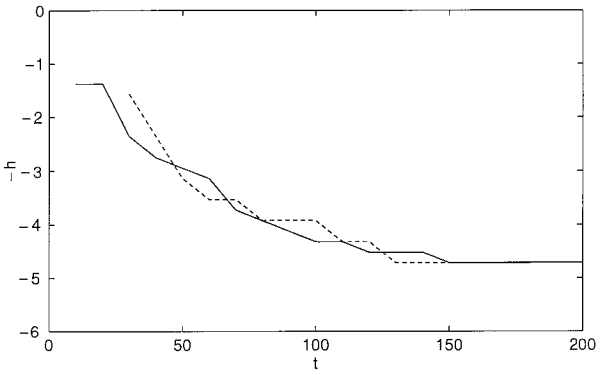

FIG. 4. Depth of the mixed layer generated by Langmuir cells in two computational boxes with $L = 2\pi$ (solid) and $L = 4\pi$ (dashed).

shown in Fig. 4 for two numerical runs with box width $\beta\tilde{L} = 2\pi$ and $\beta\tilde{L} = 4\pi$. The depth increases rapidly as Langmuir cells grow in scale and engulf water from below, but then approaches an asymptotic limit. In the quasi-steady state, two cells fill the computational box, but the cells are flat in the wider box. At small values of La in the wider box, a new instability may develop and a pair of small cells may be regenerated at the surface divergence between the two large cells, though this cell regeneration process does not appear to further deepen the mixed layer because it is confined near the surface. Figure 4 shows that almost the same cell depth is obtained for the two computational boxes with different widths. Hence $\beta\tilde{h}$ is controlled by stratification rather than by side boundaries. Further SML deepening may occur through localized shear instability and this will be discussed in section 7.

The nondimensional time taken for the SML to reach this depth is approximately $t_d = 130$, as shown in Fig. 4. Translated into dimensional units, this gives

$$\tilde{t}_d = \frac{\nu_T}{u_*^2}\left(\frac{\nu_T S_0 \beta}{u_*^2}\right)^{-1/2} t_d \tag{20}$$

$$= \frac{\nu_T}{u_*}(\nu_T S_0 \beta)^{-1/2} t_d \tag{21}$$

$$= \frac{1}{u_* \beta}\left(\frac{S_0}{u_*}\right)^{-1/3} \mathrm{La}^{1/3} t_d. \tag{22}$$

For La $= 0.01$, $u_* = 1.3 \times 10^{-3} U_w$, and with $1/(2\beta) = 0.12 U_w^2/g$ and $S_0/u_* = 5.75$ (LG93) appropriate for fully developed seas, $\tilde{t}_d \approx 3 \times 10^3 U_w/g$ or 50 min for $U_w = 10$ m s^{-1}. For developing seas $\tilde{t}_d$ may still be about the same if ν_T does not change, since $S_0\beta$ has a flat spectrum and so would not be much reduced.

4. Parameterization of the SML depth in terms of a Froude number

For a preexisting linear stratification, the depth $\tilde{h}$ of

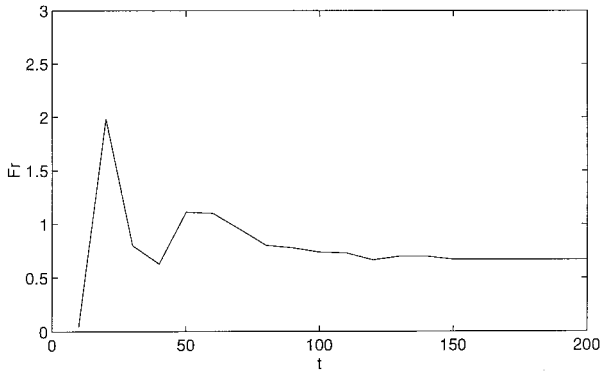

FIG. 5. Time series of Fr for La = 0.03, R_{LN} = 0.05, and Pr = 1.

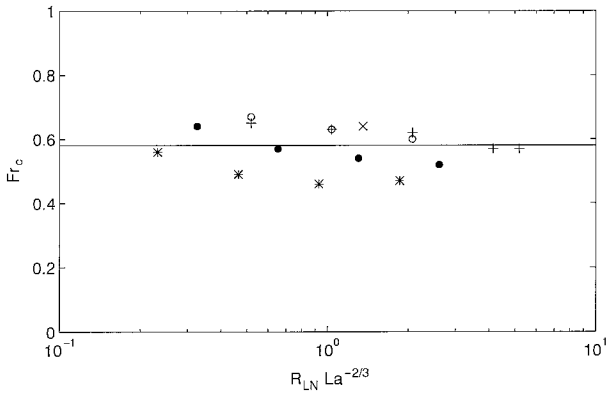

FIG. 6. Summary of critical Froude number Fr_c in La and $R_{LN}\mathrm{La}^{-2/3}$ parameter space. Symbol "*" corresponds to La = 0.1, "●" to La = 0.06, "+" to La = 0.03, and "×" to La = 0.02 at Pr = 1, while "o" corresponds to La = 0.03 at Pr = 2.

the SML produced by LC depends mainly on three dimensionless parameters La, R_{LN}, and Pr (S_w does not enter the nondimensionalized governing equations, but see later for a discussion on the effects of $\beta\tilde{h}$). Langmuir circulation generates vertical velocities with vertical penetration inhibited by stratification. The cell penetration depth $\tilde{h}$ thus depends on the competition, between vertical motion and stratification, represented by the Froude number

$$\mathrm{Fr} = \frac{\tilde{w}_{dn}}{N\tilde{h}} = \frac{w_{dn}}{R_{LN}^{1/2}h}, \tag{23}$$

where $\tilde{w}_{dn}$ and w_{dn} are the maximum dimensional and nondimensionalized downwelling velocities, respectively, generated by Langmuir cells in homogeneous water.

Figure 5 displays a time series of Fr. The Froude number is high when LC engulfs water and deepens the SML but reaches a constant value when the SML deepening is arrested. The vertical penetration is inhibited when Fr reaches a value of about 0.6.

In order for this to lead to a useful parameterization for the SML produced by LC, the critical value Fr_c should be independent of the input parameters La, R_{LN}, and Pr. Estimates of Fr_c obtained from various numerical runs are summarized in Fig. 6. When obtaining h, we have checked the influence of box width L and confirmed that the cells in the final quasi-steady state are defined by the stratification rather than by the side boundaries; for smaller $R_{LN}\mathrm{La}^{-2/3}$ (weaker stratification) the cells are larger and it is necessary to run the models in larger computational boxes. The figure suggests that Fr_c is approximately a constant for any oceanographically reasonable combination of La, R_{LN}, and Pr; namely,

$$\mathrm{Fr}_c \approx 0.6. \tag{24}$$

This has a physical interpretation in terms of kinetic energy conversion into potential energy; LC generates the kinetic energy that is used to raise water particles from their initial equilibrium positions. Penetration stops if the potential energy required ($\frac{1}{2}N^2\tilde{h}^2$) is more than the kinetic energy available ($\frac{1}{2}\tilde{w}^2$). We can also understand the LC growth and arrest in terms of angular momentum balance. The Craik–Leibovich vortex force exerts torque in the water and generates circular motions. If there were no stratification, cells would grow indefinitely, even though more slowly at later stages. In stratified water, a buoyancy torque is created, which counteracts the driving vortex force so that eventually an angular momentum balance is reached.

We note that $e^{2\beta\tilde{h}} \gg 1$, such that the vortex force that generates LC is concentrated near the surface. Although the depth at which $\tilde{w}_{dn}$ is reached remains close to the surface, the vertical velocity does not drop more rapidly with depth for large cells. In fact, the profiles of normalized downwelling velocity ($\tilde{w}/\tilde{w}_{dn}$ versus $\tilde{z}/\tilde{h}$) appear to be similar in the final quasi-steady state for various values of R_{LN}, at fixed La and Pr. This supports the idea that the maximum downwelling velocity determines the cell penetration depth independently of $\beta\tilde{h}$ when $e^{2\beta\tilde{h}} \gg 1$.

5. Incorporation of LC into the PWP model

The maximum downwelling velocity of Langmuir cells in homogeneous water can be expressed as (LG93)

$$\tilde{w}_{dn} = u_*\left(\frac{S_0}{u_*}\right)^{1/3}\mathrm{La}^{-1/3}w_{dn} \tag{25}$$

$$= 0.72\left(\frac{S_0}{u_*}\right)^{1/3}\mathrm{La}^{-1/3}u_*. \tag{26}$$

The eddy viscosity ν_T is an unknown in our model, but a choice of La = 0.01 gives

$$\tilde{w}_{dn} \approx 0.008\ U_w, \tag{27}$$

in reasonable agreement with observed downwelling velocities.

Equations (23), (24), and (26) give for the dimensional mixed layer depth

$$\tilde{h} = 1.2\frac{u_*}{N}\left(\frac{S_0}{u_*}\right)^{1/3}\mathrm{La}^{-1/3} \tag{28}$$

$$= 1.2\frac{v_*}{N}(\nu_T S_0\beta)^{-1/2}\left(\frac{S_0}{u_*}\right). \tag{29}$$

For La = 0.01 and for fully developed seas for which $S_w = (S_0/u_*) = 5.75$,

$$\tilde{h} \approx 10u_*/N. \tag{30}$$

The ratio S_w can be significantly smaller in developing seas, leading to a smaller coefficient of u_*/N in (30) if ν_T stays the same.

We can compare (30) with the results of the simple model of Pollard et al. (1973, hereafter PRT) for the upper-ocean response to an imposed wind stress. They argued that the interface is unstable due to the near discontinuity of velocity across it and suggested that the problem be closed by an assumption involving a suitable Richardson number. They hypothesized that $R_b = g\Delta\rho\tilde{h}/(\rho_0|\Delta\tilde{\mathbf{u}}^2|)$, in which $\Delta\rho$ and $|\Delta\tilde{\mathbf{u}}|$ are the velocity and density differences across the mixed layer, maintains a value of 1 during SML deepening. For an initially constant stratification they predicted the SML depth to increase with time, up to $ft = \pi$, as

$$\tilde{h} = u_*\left[\frac{4(1 - \cos ft)}{f^2N^2}\right]^{1/4}, \tag{31}$$

with the initial deepening obeying

$$\tilde{h} = 2^{1/4}u_*(t/N)^{1/2}. \tag{32}$$

After one-half inertial period, the deepening is arrested by rotation at depth, giving

$$\tilde{h}_{\max} = 2^{3/4}u_*/(Nf)^{1/2}. \tag{33}$$

Taking the Coriolis parameter $f = 10^{-4}\ \mathrm{s}^{-1}$ and the buoyancy frequency $N^2 = 10^{-5}$ to $10^{-4}\ \mathrm{s}^{-2}$, one obtains

$$\tilde{h}_{\max} = (10 \text{ to } 17)u_*/N. \tag{34}$$

In the PRT model $10u_*/N$ is obtained after a time ranging from $(0.7 \text{ to } \pi)f^{-1}$ h, generally significantly longer than the time taken for LC to reach the same depth.

To incorporate the effects of LC into a mixed layer model, we propose to use a criterion in terms of the buoyancy jump at the base, as in the bulk Richardson criterion in the PWP model (Price et al. 1986), which uses 0.65 rather than 1 as the critical value of R_b. The important difference is that our LC criterion depends on u_*, whereas the PRT or PWP criterion depends on $|\Delta\tilde{\mathbf{u}}|$. It is only for idealized problems that u_* and $|\Delta\tilde{\mathbf{u}}|$ are simply related.

To generalize, we note that our numerical simulations suggest that LC erodes an initially uniformly stratified water and creates an SML with depth $\tilde{h}$ and buoyancy jump Δb at its base. Because the heat content is conserved,

$$\Delta b = \frac{1}{2}N^2\tilde{h}. \tag{35}$$

This combines with (28) to yield

$$\Delta b = cu_*^2/\tilde{h}, \tag{36}$$

where $c = 0.72(S_0/u_*)^{2/3}\,\mathrm{La}^{-2/3} = 0.72S_0/(\nu_T\beta)$. For fully developed seas, this reduces to $c = 50$, using the same parameter values as in (22).

We thus propose that, in addition to the bulk Richardson number criterion that the SML will deepen unless

$$\Delta b \geq 0.65|\Delta\tilde{\mathbf{u}}|^2/\tilde{h}, \tag{37}$$

we also use a criterion that LC engulfment will occur unless

$$\Delta b \geq 50u_*^2/\tilde{h}, \tag{38}$$

Clearly, LC dominates the SML deepening if

$$|\Delta\tilde{\mathbf{u}}| < 9u_* = 0.01U_w, \tag{39}$$

that is, if the velocity shear across the base of the mixed layer is no greater than 1% of the wind speed.

Equation (38) appears to be similar to Kraus and Turner's (1967) entrainment model. A u_* dependence was later disputed by Price (1979), however, who proposed that the rate of entrainment be scaled instead with the velocity difference across the interface, as this resolved the disagreement between the two laboratory experiments (Kato and Phillips 1969; Kantha et al. 1977). In the Mixed Layer Experiment (MILE), Davis et al. (1981) suggested empirical deepening formulas involving both u_* and $|\Delta\tilde{\mathbf{u}}|$ and obtained better agreement with observations than with formulas depending on u_* or $|\Delta\tilde{\mathbf{u}}|$ alone. Our formula involves u_* but is based on the modeling of Langmuir circulation, and the coefficient c gives an explicit dependence on the sea state and turbulence parameterization.

To summarize the numerical results on the erosion into linear stratification by LC, we note that $\mathrm{Fr}_c \approx 0.6$ and is insensitive to input parameters La, Pr, and R_{LN} over a plausible range. However, the deeper stratification is fixed such that $R_{Lb} = R_{LN}(\beta\tilde{h})/2$. To make the deepening criterion (38) more general, we next turn to the two-layer stratification.

6. Test of the buoyancy jump criterion to SML deepening in a two-layer fluid

We consider a two-layer fluid in which two homogeneous water layers are connected by a sharp interface (see Fig. 1c). In this case $R_{LN} = 0$. Two values of $\beta\tilde{h}$ are studied. For each $\beta\tilde{h}$, we shall vary R_{Lb} across a range and determine whether the surface layer deepens according to the criterion suggested by (38). This provides a genuine test of the criterion because the deep water is homogeneous and no buoyancy force is available there to inhibit cell penetration if the buoyancy jump at the interface cannot stop the SML deepening.

The dimensional governing equations are still (1)–(4). Denoting the temperature difference across the interface by ΔT, the depth of the top layer by $\tilde{h}$, and nondimensionalizing distance, velocity, and time as (5) to (8), but scaling temperature with ΔT instead of $N^2/(\alpha g\beta)$, we obtain

$$\frac{\partial u}{\partial t} + v\frac{\partial u}{\partial y} + w\frac{\partial u}{\partial z} = \mathrm{La}\nabla^2 u, \tag{40}$$

$$\frac{\partial \Omega}{\partial t} + v\frac{\partial \Omega}{\partial y} + w\frac{\partial \Omega}{\partial z} = \mathrm{La}\nabla^2\Omega - \frac{du_s}{dz}\frac{\partial u}{\partial y} + R_{Lb}\frac{\partial \theta}{\partial y}, \tag{41}$$

$$\frac{\partial \theta}{\partial t} + v\frac{\partial \theta}{\partial y} + w\frac{\partial \theta}{\partial z} = \frac{\mathrm{La}}{\mathrm{Pr}}\nabla^2\theta, \tag{42}$$

$$v = -\frac{\partial \Psi}{\partial z}, \qquad w = \frac{\partial \Psi}{\partial y},$$

$$\Omega = \nabla^2\Psi, \tag{43}$$

where

$$R_{Lb} = \frac{\alpha g \Delta T \nu_T}{S_0 u_*^2}. \tag{44}$$

As in section 2, the downwind current is split into a mean and a perturbation. The boundary conditions to be satisfied at the top and bottom boundaries are

$$\frac{\partial u'}{\partial z} = 0, \qquad \psi = \frac{\partial^2 \psi}{\partial z^2} = 0, \qquad \frac{\partial \theta}{\partial z} = 0,$$

$$\text{at } z = 0, -\beta\tilde{d},$$

where the depth $\beta\tilde{d}$ at the lower boundary is chosen such that water in the lower portion of the box stays stagnant. The heat flux is kept equal to zero at the top and bottom boundaries, and the total heat content of the water column is thus conserved.

The initial temperature has a two-layer structure

$$\theta = \frac{1 + \tanh[\gamma(z + \beta\tilde{h})]}{2}, \tag{45}$$

in which γ measures the thickness of the initial interface. A choice of $\gamma = 20$ makes the interface thin, but the thickness increases as $2(\mathrm{Lat/Pr})^{1/2}$ due to temperature diffusion and this could potentially affect the cell penetration. To reduce this diffusion problem we choose Pr = 2 or larger.

According to (38), the surface layer should deepen if $\Delta b < 50u_*^2/\tilde{h}$. This inequality can be translated into a criterion for R_{Lb}.

Equation (36) gave

$$(\Delta b\tilde{h})_{\mathrm{cri}} = 0.72\left(\frac{S_0}{u_*}\right)^{2/3}\mathrm{La}^{-2/3}u_*^2 \tag{46}$$

for linearly stratified fluid where $(\Delta b\tilde{h})_{\mathrm{cri}}$ denotes the value of $\Delta b\tilde{h}$ at which deepening of the SML stopped. Together with (44) and noting $\Delta b = \alpha g \Delta T$, we obtain

$$\Delta b\tilde{h} = \frac{S_0 u_*^2}{\nu_T \beta} R_{Lb} h = h\left(\frac{S_0}{u_*}\right)^{2/3}\mathrm{La}^{-2/3}u_*^2 R_{Lb} = \frac{h}{0.72}(\Delta b\tilde{h})_{\mathrm{cri}} R_{Lb}, \tag{47}$$

which is rearranged to

$$R_{Lb} = \frac{0.72}{h}\frac{\Delta b\tilde{h}}{(\Delta b\tilde{h})_{\mathrm{cri}}}. \tag{48}$$

The SML should thus deepen if $\Delta b\tilde{h} < (\Delta b\tilde{h})_{\mathrm{cri}}$ or

$$R_{Lb} < 0.72/h. \tag{49}$$

Taking $\beta\tilde{h} = h = 4$, the SML should deepen if $R_{Lb} < 0.18$, whereas no rapid deepening should occur when $R_{Lb} \geq 0.18$. We have run our numerical model with a range of R_{Lb} values below and above the critical value. The SML stays at approximately the same depth for $R_{Lb} = 0.18$, 0.25, 0.3, but penetrates to an increasingly greater depth for $R_{Lb} = 0.05$, 0.1, 0.15 (Fig. 7a), though the deepening is significantly slower for bigger cells at later times. This criterion (38) has also been checked for $\beta\tilde{h} = 2$ (Fig. 7b) in which the critical value $R_{Lb} = 0.36$, although higher values of Pr are needed in order to minimize diffusion effects.

7. Enhanced shear instability beneath downwelling jets

We have shown that LC rapidly produces an SML through engulfment. Further entrainment due to shear instability is possible although the two-dimensional model, which assumes no dependence in the downwind direction, cannot resolve this. As a first step, we calculate the gradient Richardson number from the downwind current $\langle u\rangle$ and temperature $\langle\theta\rangle$ averaged across the cells for the runs that we started with linear stratification. We define this as

$$\mathrm{Ri}_{gav} = \frac{-g(\partial\langle\tilde{\rho}\rangle/\partial\tilde{z})}{\tilde{\rho}(\partial\langle\tilde{u}\rangle/\partial\tilde{z})^2} = \frac{\alpha g(\partial\langle\tilde{\theta}\rangle/\partial\tilde{z})}{(\partial\langle\ \tilde{u}\tilde{u}\rangle/\partial\tilde{z})^2} = \left(\frac{S_0}{u_*}\right)^{4/3}\mathrm{La}^{2/3}|R_{LN}|\frac{\partial\langle\theta\rangle/\partial z}{(\partial\langle u\rangle/\partial z)^2}. \tag{50}$$

A time series plotted in Fig. 8 shows that Ri_{gav} evaluated at depth $\beta\tilde{h}$ approaches 0.56 when the cells reach a quasi-steady state, indicating no shear instability. This result is misleading, however, because the downwind shear and temperature gradient are far from uniform in the crosswind direction. Figure 9 shows a variation of

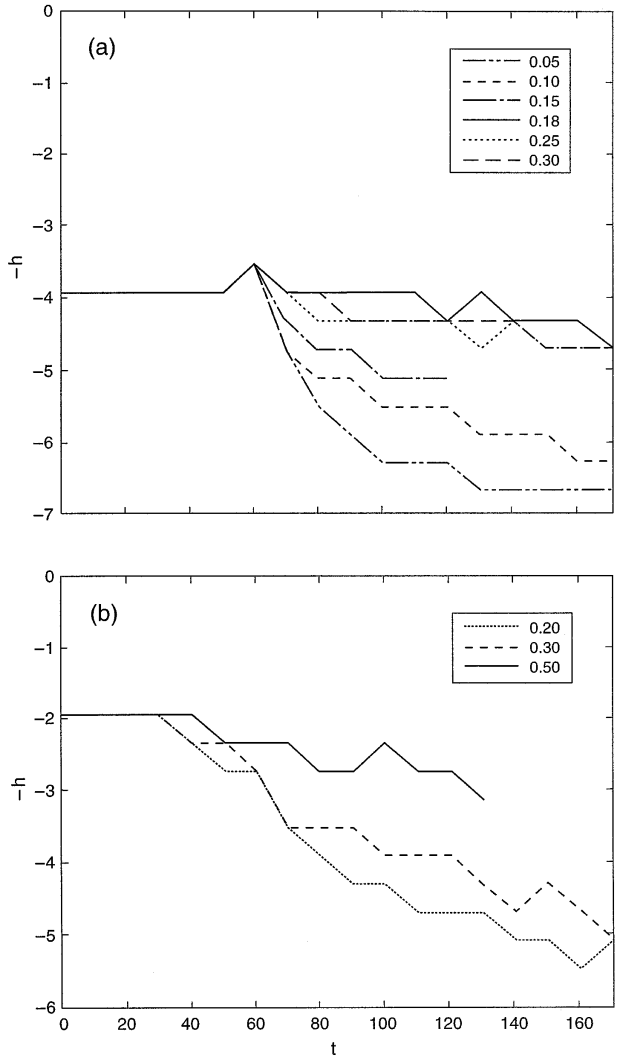

FIG. 7. Depth of the surface layer in a two-layer fluid starting (a) at $h = 4$ and for $R_{Lb} = 0.05, 0.1, 0.15, 0.18, 0.25, 0.3$, and (b) at $h = 2$ and for $R_{Lb} = 0.2, 0.3$, and 0.5. In these runs we choose La = 0.03 and Pr = 2 except that Pr = 4 is chosen for $h = 2$ and $R_{Lb} = 0.5$ in order to minimize the effects of diffusion.

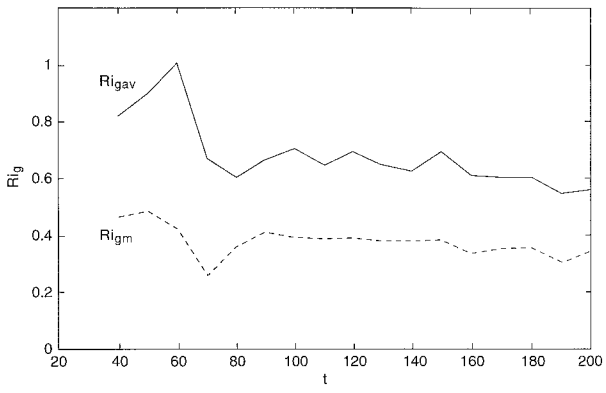

FIG. 8. Time series of gradient Richardson numbers. A value of $S_0/u_* = 5.75$ is taken in the calculations.

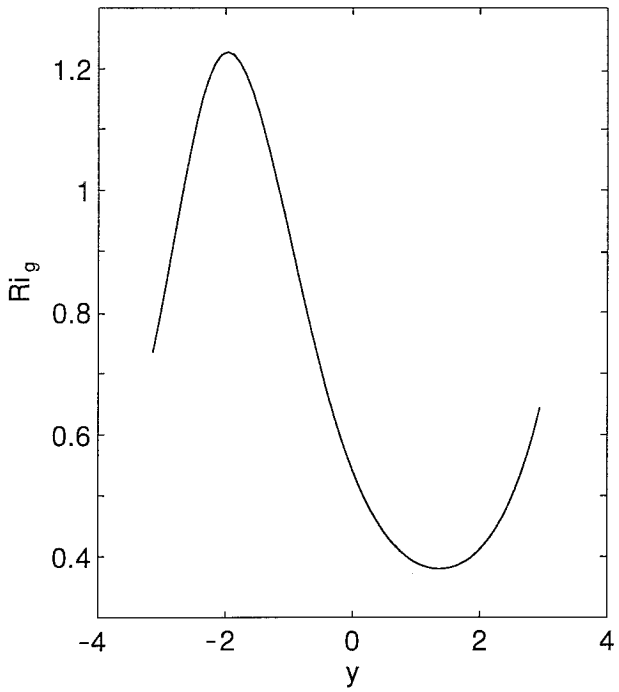

FIG. 9. The crosswind variation of Ri_g at depth h. Again we use $S_0/u_* = 5.75$.

the gradient Richardson number Ri_g along a horizontal line at depth $\beta\tilde{h}$. Evidently Ri_g exhibits considerable variability in the crosswind direction, with variation by a factor of 3. The minimum value Ri_{gm} is located beneath the surface convergence, where the downwelling jet carries fast-moving fluid down, making the shear much stronger. As shown in Fig. 8, Ri_{gm} is significantly smaller than Ri_{gav}.

Figure 10 summarizes Ri_{gm} in parameter space. We

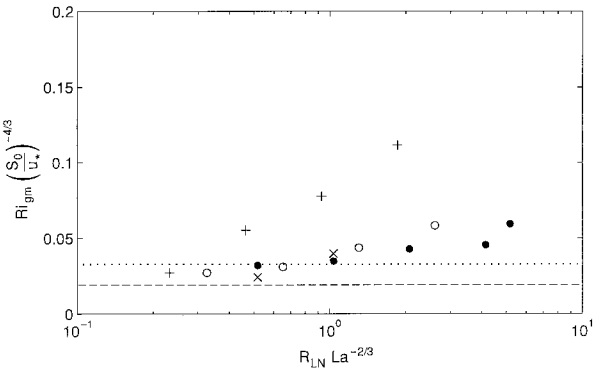

FIG. 10. Summary of minimum gradient Richardson number Ri_{gm} $(S_0/u_*)^{-4/3}$ as a function of La, $(R_{LN}\mathrm{La}^{-2/3})$ and Pr. Symbol "+" corresponds to La = 0.1, "o" to La = 0.06, and "●" to La = 0.03 at Pr = 1, while "×" corresponds to La = 0.03 and Pr = 2. The critical value $\mathrm{Ri}_g = 0.25$ becomes a narrow band in $\mathrm{Ri}_g(S_0/u_*)^{-4/3}$ because $S_0/u_* = 4.6$ to 6.9.

observe a trend that Ri_{gm} decreases with decreasing $(R_{LN}\mathrm{La}^{-2/3})$; when the water is less stratified, Ri_{gm} becomes smaller. The two curves corresponding to La = 0.06 and La = 0.03 are close to each other, indicating that establishing the condition for shear instability is not sensitive to the eddy viscosity. Figure 10 suggests the likelihood of shear instability for $0.1 < (R_{LN}\mathrm{La}^{-2/3}) < 1$, although Ri_{gm} appears to be only marginally less than 0.25.

In this discussion of the gradient Richardson number, we have only considered the velocity and temperature associated with LC eroding an initially linear stratification. In reality, horizontal currents due to previous wind events and the Coriolis force may exist and should be considered. Overall, it is worth pointing out that, when LC is present, further SML deepening may be caused by enhanced shear instability beneath downwelling jets. Incorporating this into one-dimensional SML models will require further work.

8. Conclusions

We have demonstrated that LC causes a rapid deepening of SML to a depth $\tilde{h} \approx 10u_*/N$ for initially linear stratification in fully developed seas. The estimate is derived from the Froude number criterion $\mathrm{Fr} = \tilde{w}_{dn}/(N\tilde{h})$, which is found to be a constant of about 0.6. The formula for $\tilde{h}$ can also be understood from dimensional arguments. Langmuir circulation is driven by u_* and the stratification is represented by N. The depth $\tilde{h}$ depends on these two quantities and, if $\nu_T \propto u_*^3/g$ and $\beta \propto g/u_*^2$, the only dimensionally consistent statement is $\tilde{h} = cu_*/N$ in which c is a constant of proportionality. For fully developed seas, $c \approx 10$. For developing seas S_0/u_* can be significantly smaller and c may be less than 10. Equivalently, and more generally, the buoyancy jump at the base of the mixed layer is predicted to be about $50u_*^2/\tilde{h}$, less for developing seas. This buoyancy jump criterion (38), and that of PWP (37), have been tested against oceanic observations, which show some evidence of mixed layer deepening due to LC (Li et al. 1995).

The model predicts that both $\tilde{h}$ and $\tilde{w}_{dn}$ vary like $\nu_T^{1/2}$ [from the $\mathrm{La}^{-1/3}$ dependence of (26) and (28)], depending on the magnitude of eddy viscosity. Representing the effects of turbulence by a constant eddy viscosity requires further examination, and recent LES (large eddy simulation) studies (Skyllingstad and Denbo 1995) show some promise of eliminating the need for this parameterization. However, we must emphasize that the parameterization of the SML depth in terms of Fr is independent of La. It should be possible to deduce a similar parameterization in LES models that could also resolve the shear instability, which we have shown beneath downwelling jets.

We have used the two-dimensional Craik–Leibovich model in this paper. Future work will need to consider three-dimensional effects. Using sidescan sonar to image the ocean surface, Farmer and Li (1995) observed that bubble clouds collected at the convergence zones of Langmuir circulation produce parallel lines at low wind speeds but organize into Y-shaped patterns at high winds. In a recent investigation of a three-dimensional model of Langmuir circulation, Tandon and Leibovich (1995) found considerable levels of spatial and temporal complexity in the flows. The 3D LES simulations by Skyllingstad and Denbo (1995) and McWilliams et al. (1996) have also shown the Y-shaped patterns in the contour plots of vertical velocity. It should be possible to use a 3D LES model to derive a more robust and realistic parameterization of Langmuir circulation in the deepening of the ocean surface layer.

Acknowledgments. We thank Konstantin Zahariev, Al Plueddemann, Bob Stewart, and Eric D'Asaro for useful discussions. We also thank Bob Weller, Sid Leibovich, and two anonymous referees for helpful comments on a draft of this paper. Rosalie Rutka helped prepare the diagrams. Financial support from Canada's Natural Sciences and Engineering Research Council and the U.S. Office of Naval Research is gratefully acknowledged.

REFERENCES

Craik, A. D. D., 1977: The generation of Langmuir circulations by an instability mechanism. *J. Fluid Mech.,* **81,** 209–223.

Davis, R. E., R. deSzoeke, and P. Niiler, 1981: Variability in the upper ocean during MILE. Part II: Modeling the mixed layer response. *Deep-Sea Res.,* **28A,** 1453–1475.

Farmer, D. M., and M. Li, 1995: Patterns of bubble clouds organized by Langmuir circulation. *J. Phys. Oceanogr.,* **25,** 1426–1440.

Kantha, L. H., O. M. Phillips, and R. S. Azad, 1977: On turbulent entrainment at a stable interface. *J. Fluid Mech.,* **79,** 753–768.

Kato, H., and O. M. Phillips, 1969: On the penetration of a turbulent layer into stratified fluid. *J. Fluid Mech.,* **37,** 643–665.

Kraus, E. B., and J. S. Turner, 1967: A one-dimensional model of the seasonal thermocline. Part II. The general theory and its consequences. *Tellus,* **19,** 98–105.

Langmuir, I., 1938: Surface motion of water induced by wind. *Science,* **87,** 119–123.

Large, W. G., J. C. McWilliams, and S. C. Doney, 1994: Oceanic vertical mixing: A review and a model with a nonlocal K-profile boundary layer parameterization. *Rev. Geophys.,* **32,** 363–403.

Leibovich, S., 1977: Convective instability of stably stratified water in the ocean. *J. Fluid Mech.,* **82,** 561–581.

——, 1983: The form and dynamics of Langmuir circulations. *Annu. Rev. Fluid Mech.,* **15,** 391–427.

——, and S. Paolucci, 1980: The Langmuir circulation instability as a mixing mechanism in the upper ocean. *J. Phys. Oceanogr.,* **10,** 186–207.

Lele, S. K., 1985: Some problems of hydrodynamic stability arising in geophysical fluid dynamics. Ph.D. dissertation, Cornell University, 302 pp.

Li, M., and C. Garrett, 1993: Cell merging and jet/downwelling ratio in Langmuir circulation. *J. Mar. Res.,* **51,** 737–769.

——, and ——, 1995: Is Langmuir circulation driven by surface waves or surface cooling? *J. Phys. Oceanogr.,* **25,** 64–76.

——, K. Zahariev, and C. Garrett, 1995: Role of Langmuir circulation

in the deepening of the ocean surface mixed layer. *Science,* **270,** 1955–1957.

McWilliams, J. C., P. P. Sullivan, and C.-H. Moeng, 1996: Langmuir turbulence in the ocean. *J. Fluid Mech.,* in press.

Mellor, G. L., and T. Yamada, 1974: A hierarchy of turbulence closure models for planetary boundary layers. *J. Atmos. Sci.,* **31,** 1791–1806.

——, and ——, 1982: Development of a turbulence closure model for geophysical fluid problems. *Rev. Geophys. Space Phys.,* **20,** 851–875.

Niiler, P. P., and E. B. Kraus, 1977: One-dimensional models of the upper ocean. *Modeling and Prediction of the Upper Layers of the Ocean.,* E. B. Kraus, Ed., Pergamon, 143–172.

Pollard, R. T., P. B. Rhines, and R. O. R. Y. Thompson, 1973: The deepening of the wind-mixed layer. *Geophys. Fluid Dyn.,* **3,** 381–404.

Price, J. F., 1979: On the scaling of stress-driven entrainment experiments. *J. Fluid Mech.,* **90,** 509–529.

——, R. A. Weller, and R. Pinkel, 1986: Diurnal cycling: Observations and models of the upper ocean response to diurnal heating, cooling and wind mixing. *J. Geophys. Res.,* **91,** 8411–8427.

Skyllingstad, E. D., and D. W. Denbo, 1995: An ocean large eddy simulation of Langmuir circulations and convection in the surface mixed layer. *J. Geophys. Res.,* **100,** 8501–8522.

Tandon, A., and S. Leibovich, 1995: Simulations of three-dimensional Langmuir circulation in water of constant density. *J. Geophys. Res.,* **100,** 22 613–22 623.

Thorpe, S. A., 1985: Small-scale processes in the upper ocean boundary layer. *Nature,* **318,** 519–522.

——, 1992: Bubble clouds and the dynamics of the upper ocean. *Quart. J. Roy. Meteor. Soc.,* **118,** 1–22.

Weller, R. A., and J. F. Price, 1988: Langmuir circulation within the oceanic mixed layer. *Deep-Sea Res.,* **35,** 711–747.